

# Two-neutron knockout from neutron-deficient $^{34}\text{Ar}$ , $^{30}\text{S}$ , and $^{26}\text{Si}$

K. Yoneda,<sup>1,\*</sup> A. Obertelli,<sup>1</sup> A. Gade,<sup>1,2</sup> D. Bazin,<sup>1</sup> B. A. Brown,<sup>1,2</sup> C. M. Campbell,<sup>1,2</sup> J. M. Cook,<sup>1,2</sup> P. D. Cottle,<sup>3</sup> A. D. Davies,<sup>1,2</sup> D.-C. Dinca,<sup>1,2,†</sup> T. Glasmacher,<sup>1,2</sup> P. G. Hansen,<sup>1,2</sup> T. Hoagland,<sup>1</sup> K. W. Kemper,<sup>3</sup> J.-L. Lecouey,<sup>1,‡</sup> W. F. Mueller,<sup>1</sup> R. R. Reynolds,<sup>3</sup> B. T. Roeder,<sup>3</sup> J. R. Terry,<sup>1,2</sup> J. A. Tostevin,<sup>4</sup> and H. Zwahlen<sup>1,2</sup>

<sup>1</sup>National Superconducting Cyclotron Laboratory, Michigan State University, East Lansing, MI 48824

<sup>2</sup>Department of Physics and Astronomy, Michigan State University, East Lansing, MI 48824

<sup>3</sup>Department of Physics, Florida State University, Tallahassee, FL 32306

<sup>4</sup>Department of Physics, School of Electronics and Physical Sciences, University of Surrey, Guildford, Surrey GU2 7XH, United Kingdom

(Dated: October 6, 2018)

Two-neutron knockout reactions from nuclei in the proximity of the proton dripline have been studied using intermediate-energy beams of neutron-deficient  $^{34}\text{Ar}$ ,  $^{30}\text{S}$ , and  $^{26}\text{Si}$ . The inclusive cross sections, and also the partial cross sections for the population of individual bound final states of the  $^{32}\text{Ar}$ ,  $^{28}\text{S}$  and  $^{24}\text{Si}$  knockout residues, have been determined using the combination of particle and  $\gamma$ -ray spectroscopy. Similar to the two-proton knockout mechanism on the neutron-rich side of the nuclear chart, these two-neutron removal reactions from already neutron-deficient nuclei are also shown to be consistent with a direct reaction mechanism.

Over the past decade, direct one-nucleon knockout reactions from fast beams [1] have been developed into a versatile tool applicable to structure studies of atomic nuclei beyond the valley of  $\beta$  stability. The technique has been used successfully to derive single-particle spectroscopic strengths and assign orbital angular momenta, to probe shell closures, and to study halo nuclei as well as correlation effects beyond effective-interaction theory [2, 3, 4, 5, 6, 7, 8, 9, 10, 11, 12, 13, 14, 15, 16]. The associated formalisms, used to calculate single-particle cross sections and to deduce spectroscopic factors and orbital angular momenta, employ few-body reaction theory in eikonal approximation [17] and modern shell-model and Hartree-Fock calculations [18, 19, 20]. For several well-studied cases, results from intermediate-energy knockout reactions have been shown to be consistent with information obtained from alternative approaches [21].

Two-proton knockout from neutron-rich nuclei has recently been shown to proceed as a direct reaction [22]. In that first reported experiment, two protons were removed from secondary beams of neutron-rich  $^{28}\text{Mg}$ ,  $^{30}\text{Mg}$ , and  $^{34}\text{Si}$  using a thick  $^9\text{Be}$  target. The reaction mechanism, involving sudden, peripheral collisions, is advantageous for the study of exotic nuclei since, for a given incoming beam, the residue from two-proton knockout is even more neutron-rich than that produced by one-proton removal, but with still manageable cross sections. The method has also been applied to study the very exotic nuclei  $^{42}\text{Si}$  and  $^{44}\text{S}$  [23]. A first theoretical description of the reaction process considered the stripping of two uncorrelated nucleons [22]. The correlations between the two removed nucleons within the initial nucleus have recently been incorporated via shell-model two-nucleon amplitudes [24]. These correlations were found to have a significant influence on the stripping partial cross sections to different final states, indicating that two-nucleon knockout reactions offer promise for accessing nuclear-structure infor-

mation for very exotic nuclei and probe two-nucleon correlation effects in asymmetric regimes [24].

Experiments have, so far, employed only two-proton knockout on the neutron-rich side of the nuclear chart. The present experiment provides the first measurements of two-neutron knockout from proton-rich nuclei. We report first results from the two-neutron removal reactions  $^9\text{Be}(^{34}\text{Ar}, ^{32}\text{Ar})\text{X}$ ,  $^9\text{Be}(^{30}\text{S}, ^{28}\text{S})\text{X}$  and  $^9\text{Be}(^{26}\text{Si}, ^{24}\text{Si})\text{X}$  in the proximity of the proton dripline. These nuclei were chosen since (i) the respective projectiles and knockout residues are expected to be well described by shell-model calculations within the  $sd$  shell, and (ii) the proton-to-neutron asymmetry in these nuclei strongly favors a direct two-nucleon removal reaction mechanism. *A priori*, two-nucleon removal reactions are expected to have both a direct and a multi-step component. However, the importance of the latter will depend strongly upon the thresholds for nucleon emission. For illustration, we consider the  $^{34}\text{Ar}$  projectile where the dominant two-step, two-neutron removal would involve neutron evaporation from highly excited states in  $^{33}\text{Ar}$  (Fig. 1) formed by single-nucleon removal. However, due to the neutron-deficiency of  $^{33}\text{Ar}$ , the proton evaporation channel opens first and neutron evaporation leading to  $^{32}\text{Ar}$  will be suppressed ( $S_p(^{33}\text{Ar}) = 3.3 \text{ MeV} \ll S_n(^{33}\text{Ar}) = 15.3 \text{ MeV}$ ). The same considerations apply to  $^{30}\text{S}$  and  $^{26}\text{Si}$ . Similar arguments were applied in the work of Bazin *et al.* [22].

The projectiles of interest –  $^{34}\text{Ar}$ ,  $^{30}\text{S}$  and  $^{26}\text{Si}$  – were produced by fragmentation of a 150 MeV/nucleon  $^{36}\text{Ar}$  primary beam provided by the Coupled Cyclotron Facility of the National Superconducting Cyclotron Laboratory (NSCL) at Michigan State University. The  $^9\text{Be}$  production target was located at the mid-acceptance target position of the A1900 fragment separator [25]. The beam impinged on a 376 mg/cm<sup>2</sup>  $^9\text{Be}$  secondary target located at the pivot point of the high-resolution, large-acceptance S800 magnetic spectrograph [26]. The average mid-target

energies of the beams were 110 MeV/nucleon for  $^{34}\text{Ar}$ , 111 MeV/nucleon for  $^{30}\text{S}$  and 109 MeV/nucleon for  $^{26}\text{Si}$ . Incoming particles and reaction products were unambiguously identified on an event-by-event basis. The incident particles were characterized via their time-of-flight (ToF) taken between two beam-monitoring scintillators before the target (30 meters apart). The identification of the reaction residues was performed with the detection system of the S800 focal plane: the energy loss ( $\Delta E$ ) in the ionization chamber and the ToF measured between the object point and the focal plane of the spectrograph. The time-of-flight information was corrected for the flight-path difference of the various reaction residues using the angle information provided by the position-sensitive cathode-readout drift chambers (CRDCs) [26] of the S800 focal plane. As an example, the  $\Delta E$ -ToF particle identification of  $^{24}\text{Si}$  knockout residues in the focal plane is shown in Fig. 2.

The inclusive cross sections for the two-neutron knockout to all bound final states of  $^{32}\text{Ar}$ ,  $^{28}\text{S}$  and  $^{24}\text{Si}$  were derived from the ratio of detected knockout fragments in the S800 focal plane relative to the number of incoming projectiles per number density of the  $^9\text{Be}$  target. Corrections for the finite acceptance of the spectrograph did not exceed 15%. Systematic uncertainties arise from the particle-identification gate ( $\sim 5\%$ ), purity and stability of the incoming beam ( $< 5\%$ ) and acceptance corrections ( $< 10\%$ ). These uncertainties have been added in quadrature to the statistical errors.

The reaction mechanism has been probed via the parallel-momentum distributions of the ejectiles measured in the S800 focal plane. The momentum distributions were reconstructed from the known magnetic rigidity of the spectrometer and the positions of the particles measured with the CRDCs. The parallel-momentum distribution of the  $^{24}\text{Si}$  reaction residues is shown in Fig. 3 and compared to theoretical calculations for the knock-

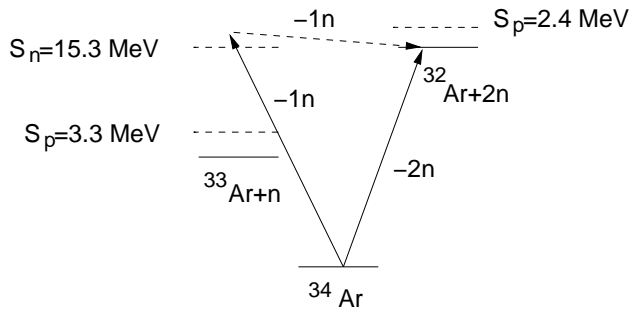


FIG. 1: Energy thresholds of the direct and two-step processes in the  $^9\text{Be}(^{34}\text{Ar}, ^{32}\text{Ar})X$  two-neutron removal reaction. The two-step process would involve neutron evaporation from  $^{33}\text{Ar}$ , but this channel is strongly suppressed since the proton separation energy  $S_p$  is much lower than the neutron separation energy  $S_n$ . Therefore, the two-neutron knockout from  $^{34}\text{Ar}$  to  $^{32}\text{Ar}$  proceeds predominantly as a direct reaction.

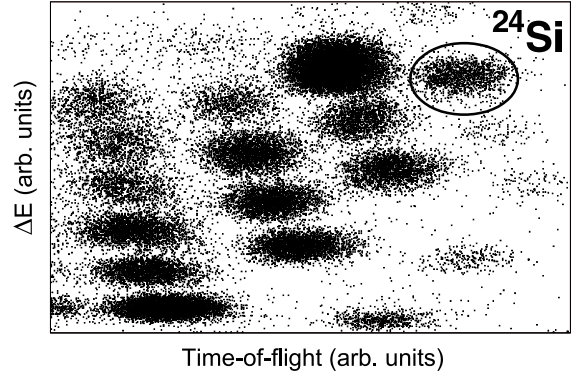


FIG. 2: Energy-loss vs. time-of-flight identification of the reaction residues detected in the S800 focal plane for incoming  $^{26}\text{Si}$  projectiles. The ToF is corrected for the ion's flight path employing the angle information obtained from the CRDC detectors in the S800 focal plane.

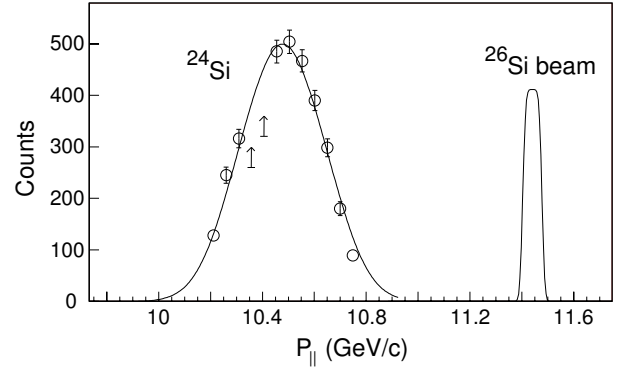


FIG. 3: Inclusive parallel-momentum distribution for  $^{24}\text{Si}$  residues from  $^{26}\text{Si}$  incoming particles. The solid line indicates the theoretical distribution for the removal of two uncorrelated neutrons, each with  $\ell = 2$ , convoluted with the experimental momentum spread of the  $^{26}\text{Si}$  beam (shown on the right). The two data points indicated by lower-limit arrows result from a damaged electronics chip (confined to a few channels) in one of the position-sensitive detectors in the S800 focal plane.

out of two neutrons, each with angular momentum  $\ell = 2$ . The two experimental points shown as arrows (in the low-momentum half of the distribution) correspond to a few channels where one of the two CRDCs was not read out properly during the experiment. The assumptions made in the theoretical calculation are the same as in [22]: the neutrons are considered to be uncorrelated and so the momentum distribution for the two-neutron knockout is the convolution of the momentum distributions from removal of each of the  $\ell=2$  neutrons. The theoretical calculation has also been convoluted with the experimental momentum spread of the incoming beam ( $\sim 1\%$ ). This comparison shows that the theory is in good agreement with the experimental distribution of the two-nucleon knockout residues. For one-nucleon removal

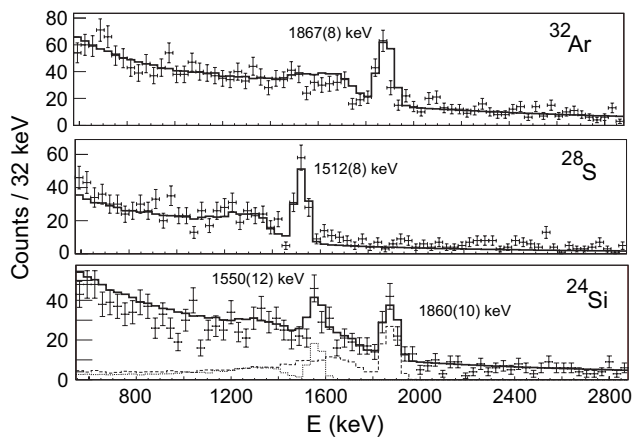


FIG. 4:  $\gamma$ -ray spectra reconstructed event-by-event into the rest frame of the emitting nucleus, in coincidence with  $^{32}\text{Ar}$ ,  $^{28}\text{S}$  and  $^{24}\text{Si}$  residues. Statistical error bars are indicated. The solid line is the result of a GEANT [29] simulation. For  $^{24}\text{Si}$ , the simulated response for the two photopeaks is shown separately in dashed and dotted lines.

reactions, the parallel-momentum distribution of knockout residues is used to assign the  $\ell$ -value of the removed nucleon. In two-nucleon knockout reactions, the parallel-momentum distributions for different  $\ell$ -values can be too similar to provide a clear assignment of the orbital angular momentum.

Cross sections to individual excited states were measured using particle- $\gamma$  coincidences. The target was surrounded by the SeGA [27], an array of seventeen 32-fold segmented high-purity Germanium detectors arranged in two rings as described in [28]. The event-by-event Doppler-corrected  $\gamma$ -ray spectra for the  $^{32}\text{Ar}$ ,  $^{28}\text{S}$  and  $^{24}\text{Si}$  residues are presented in Fig. 4. The Doppler correction has been performed by taking into account the average velocity of the projectile at the time of the  $\gamma$ -ray emission. Although an anisotropic angular distribution is expected, due to alignment effects in the knockout reaction, we assume that this can be neglected in the evaluation of the intensities. The smallness of this correction is tied to the beam energy and to the particular choice of laboratory angles for the  $\gamma$ -ray detectors ( $37^\circ$  and  $90^\circ$ ) in this experiment; see the example worked out in Fig. 12 of Ref. [1] for one-nucleon knockout.

In the case of  $^{32}\text{Ar}$  ( $S_p = 2.4$  MeV), only one  $\gamma$ -ray transition is observed at 1867(8) keV corresponding to the decay of the first  $2^+$  excited state. The measured energy is slightly different from the energy of 1824(12) keV reported in [30] using a scintillator array. We obtain an inclusive cross section of  $\sigma = 0.48(6)$  mb for the two-neutron knockout and a 0.07(4) mb cross section to the first  $2^+$  excited state. Assuming no other bound excited states, the ground state is fed directly with a cross section of 0.41(7) mb.

For  $^{28}\text{S}$  ( $S_p = 2.46(3)$  MeV), a new transition has been

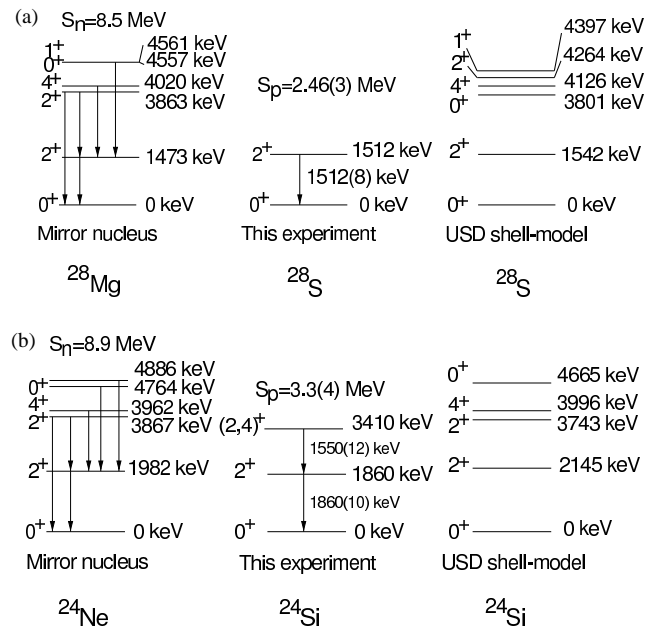


FIG. 5: Level schemes of  $^{28}\text{S}$  (a) and  $^{24}\text{Si}$  (b). The experimental results (center) are compared to shell-model predictions and to the level scheme of the respective mirror nucleus.

observed at 1512(8) keV. This transition is assigned to the decay of the first  $2^+$  state of  $^{28}\text{S}$ , based on shell-model calculations and comparison to the mirror nucleus. A shell-model calculation with the Oxbash code [31] and the USD interaction [32] predicts the first  $2^+$  state at 1543 keV excitation energy, while that of the mirror nucleus,  $^{28}\text{Mg}$ , is at 1473 keV (see Fig. 5(a)). The inclusive cross section for the production of  $^{28}\text{S}$  from  $^{30}\text{S}$  is  $\sigma = 0.73(8)$  mb. The  $2^+$  excited state is populated with a 0.34(8) mb cross section leaving a 0.39(8) mb cross section for the knockout to the ground state.

Of the three nuclei studied,  $^{24}\text{Si}$  is the most strongly bound with a proton separation energy of  $S_p = 3.3(4)$  MeV. Two  $\gamma$ -ray transitions are observed, at 1550(12) keV and 1860(10) keV, the latter being about twice as intense as the former. The observed transitions correspond to the decay of the two previously reported excited states of  $^{24}\text{Si}$  at 3441(10) keV and 1879(11) keV [33], respectively. The statistics are too low to allow a  $\gamma$ - $\gamma$  coincidence study of these two transitions. The mirror nucleus  $^{24}\text{Ne}$  exhibits a vibrator-like excitation scheme with a first  $2^+$  state lying at 1981.6(4) keV and a  $(2^+, 4^+)$  doublet at 3867(8) keV and 3962(18) keV [34], respectively. Each state of the doublet decays with an almost 100% branch to the first excited state. A comparison with  $^{24}\text{Ne}$  suggests that the two lines observed for  $^{24}\text{Si}$  in the present work are in coincidence with the first  $2^+$  state at 1860(10) keV and a  $(2,4)^+$  level at 3410(16) keV. The resulting level scheme is shown in Fig. 5 (for a discussion on mirror asymmetry in these nuclei see [35]).

TABLE I: Spin, excitation energy of the final states, and experimental cross sections for the two-neutron knockout reactions  ${}^9\text{Be}({}^{34}\text{Ar}, {}^{32}\text{Ar})\text{X}$ ,  ${}^9\text{Be}({}^{30}\text{S}, {}^{28}\text{S})\text{X}$  and  ${}^9\text{Be}({}^{26}\text{Si}, {}^{24}\text{Si})\text{X}$ . The results are compared to the theoretical cross sections which are broken down according to contributions from stripping, stripping-diffraction and diffraction. For comparison, the inclusive cross sections from the two-proton knockout reactions  ${}^9\text{Be}({}^{34}\text{Si}, {}^{32}\text{Mg})\text{X}$ ,  ${}^9\text{Be}({}^{30}\text{Mg}, {}^{28}\text{Ne})\text{X}$  and  ${}^9\text{Be}({}^{28}\text{Mg}, {}^{26}\text{Ne})\text{X}$  [22] are also presented.

Proj.	$J_f^\pi$	$E_{\text{exp}}^*$ (keV)	$\sigma_{\text{exp}}$ (mb)	$\sigma_{\text{th}}$ (mb)	str (%)	str-diff (%)	diff (%)
${}^{34}\text{Ar}$	$0_{gs}^+$	0	0.41(7)	0.71	54	39	7
	$2^+$	1867(8)	0.07(4)	0.35	51	41	8
	inclusive		0.48(6)	1.06			
${}^{30}\text{S}$	$0_{gs}^+$	0	0.39(8)	0.84	55	38	7
	$2^+$	1512(8)	0.34(8)	0.69	59	36	5
	inclusive		0.73(8)	1.54			
${}^{26}\text{Si}$	$0_{gs}^+$	0	0.71(9)	1.30	55	39	7
	$2_1^+$	1860(10)	0.15(4)	0.30	60	35	5
	$(4_1, 2_2)^+$	3410(16)	0.14(4)	0.30	61	34	5
	inclusive		1.01(10)	1.90			
Inclusive two-proton removal cross sections from [22]							
${}^{34}\text{Si}$		inclusive	0.76(10)				
${}^{30}\text{Mg}$		inclusive	0.49(5)				
${}^{28}\text{Mg}$		inclusive	1.50(10)				

Within the energy resolution of the present setup, there is no indication of a doublet at around 1550 keV.

Our experimental results are summarized in Table I. The measured inclusive and partial cross sections are given. For comparison, we also include the inclusive cross sections for the two-proton removal reactions reported in [22]. The different reactions show cross sections of the order of 1 mb for two-proton (two-neutron) knockout from neutron-rich (neutron-deficient) nuclei in the  $sd$ -shell.

Our theoretical calculations of the two-neutron-removal cross sections follow the formalism and notation of Ref. [24], which developed a full treatment of the two-nucleon stripping (absorption) cross section,  $\sigma_{\text{str}}$ . Here, we also include a full calculation of contributions to the cross sections from events where only one of the nucleons is stripped (absorbed) and the second is removed by an elastic collision (diffraction of the nucleons or residue) with the target. This is denoted  $\sigma_{\text{str-diff}}$ . We only estimate the small cross section,  $\sigma_{\text{diff}}$ , from events in which both of the tightly-bound nucleons are removed by elastic dissociation.

The two knocked-out nucleons are assumed to be removed from a set of active and partially occupied single-particle orbitals  $\phi_j$ , with spherical quantum numbers  $n(\ell j)m$ . The assumed two-nucleon overlap function, of the initial state  $J$  with each residue final state  $f$ , is denoted by  $\Psi_{JM}^{(f)}$  [24]. In the eikonal model of the direct reaction dynamics, the  $(A-2)$ -body residue (or core)

is a spectator and is assumed to interact at most elastically with the target. It thus enters the formalism through a residue-target elastic transmission probability  $|\mathcal{S}_c|^2$ . Events in which a nucleon is absorbed are described by the nucleon-target absorption probabilities  $[1 - |\mathcal{S}_i|^2]$ . The  $\mathcal{S}$  and  $\phi_j$  are calculated as discussed in Ref. [14], being constrained by Hartree-Fock systematics.

Contributions to the two-nucleon knockout cross section from the diffractive removal of one nucleon, say 1, and absorption of the second, 2, are included in the expression

$$\sigma_1 = \frac{1}{2J+1} \sum_M \int d\vec{b} \langle \Psi_{JM}^{(f)} | |\mathcal{S}_c|^2 |\mathcal{S}_1|^2 [1 - |\mathcal{S}_2|^2] | \Psi_{JM}^{(f)} \rangle, \quad (1)$$

and similarly for diffraction of nucleon 2. However, as currently stated, Eq. (1) includes events in which nucleon 1 remains bound to the residue. These single-nucleon removal events, populating bound  $(A-1)$ -body residues, must be removed by projecting off the nucleon-residue bound states, by replacing in Eq. (1)

$$|\mathcal{S}_1|^2 \rightarrow \mathcal{S}_1^* \left[ 1 - \sum_{j''m''} |\phi_{j''}^{m''}\rangle \langle \phi_{j''}^{m''}| \right] \mathcal{S}_1. \quad (2)$$

Here the sum is over the bound eigenstates  $n(\ell''j'')m''$  of nucleon 1 and the core and we use the bra-kets  $(..|$  and  $|..)$  to indicate states and integration over this nucleon's coordinates. We include all the active single particle orbitals in this sum. After having made this replacement then  $\sigma_{\text{str-diff}} = \sigma_1 + \sigma_2$ .

We only estimate the cross section from removal of both tightly-bound nucleons by elastic dissociation. We make use of the reduction in the removal cross section when one nucleon is dissociated rather than stripped, i.e.  $\sigma_i/\sigma_{\text{str}}$  as calculated above. We thus estimate the two-nucleon diffractive cross section to be  $\sigma_{\text{diff}} \approx [\sigma_i/\sigma_{\text{str}}]^2 \sigma_{\text{str}}$ . Since, see Table I,  $\sigma_i/\sigma_{\text{str}} \approx 0.35 - 0.4$ , we estimate that  $\sigma_{\text{diff}}$  makes a contribution of only 6 – 8% to the two-nucleon removal partial cross sections. Finally, the theoretical cross sections are the sum  $\sigma_{\text{th}} = \sigma_{\text{str}} + \sigma_{\text{str-diff}} + \sigma_{\text{diff}}$ . For all of the three systems studied these  $\sigma_{\text{th}}$  overpredict the measured cross sections by about a factor of two, requiring an empirical suppression of the two-neutron shell model strengths. This reduction - somewhat analogous to the suppressions observed in single-nucleon removal reactions - will be discussed elsewhere [36].

The observed differences in the cross sections to individual final states suggests (i) significant sensitivity of the reaction to the single-particle structures of the projectiles and residues, and thus (ii) that the direct two-nucleon removal mechanism provides opportunities to probe aspects of nuclear structure far from stability. Figure 6 shows the ground-state transition branching ratios,  $B_0 = \sigma(0^+)/\sigma_{\text{incl}}$ , of the three two-neutron removal reactions. The measured  $B_0$  are compared to two model

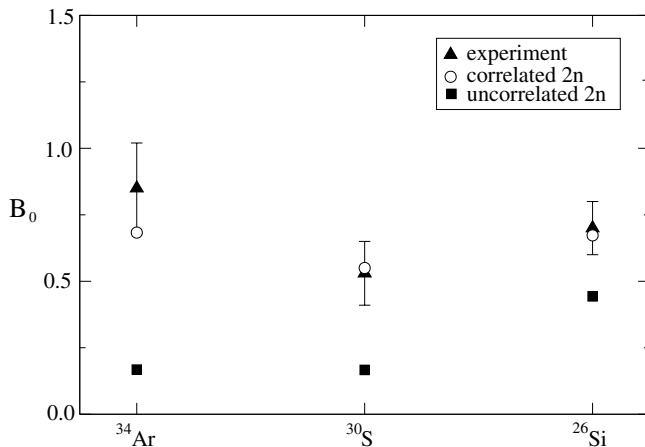


FIG. 6: Ground state branching ratios  $B_0 = \sigma(0^+)/\sigma_{\text{incl}}$  in the two-neutron removal reactions from  $^{26}\text{Si}$ ,  $^{30}\text{S}$  and  $^{34}\text{Ar}$  from (i) the experiment, (ii) calculated assuming the removal of two uncorrelated neutrons, and (iii) when including correlations via the many-body shell model wave functions [24, 36].

calculations. The first assumes the knockout of two completely uncorrelated neutrons from pure configurations  $\nu[d_{5/2}]^4$ ,  $B_0=4/9$ ,  $\nu[d_{5/2}]^6$ ,  $B_0=1/6$ , and  $\nu[d_{5/2}]^6[s_{1/2}]^2$ ,  $B_0\approx 1/6$ , for  $^{26}\text{Si}$ ,  $^{30}\text{S}$  and  $^{34}\text{Ar}$ , respectively (see e.g. Section III of [24]). The second calculation includes fully the pairing correlations between the neutrons as given by the many-body,  $sd$ -shell model wave functions [24, 36]. The experimental branching ratios are in agreement with the model for removal of two correlated neutrons while the uncorrelated neutrons assumption fails to reproduce the data. Specifically, these direct two-neutron knockout reactions show sensitivity to, and insight into the pair-correlations of the two neutrons, leading to an enhanced  $0^+$  cross section. Unlike one-nucleon knockout reactions, here the two-particle shell-model components contribute coherently for a given total angular momentum, resulting in interference effects. This strong interplay between nuclear structure and the reaction dynamics is evident in the results in Table I and Fig. 6.

In summary, two-neutron knockout reaction measurements have been performed on the already neutron-deficient nuclei  $^{34}\text{Ar}$ ,  $^{30}\text{S}$ , and  $^{26}\text{Si}$ , near the proton dripline. Particle- $\gamma$  coincidences allowed the measurement of the partial cross sections to individual bound final states. Level schemes of the residues are proposed using comparisons with the mirror nuclei and with USD shell-model calculations. The inclusive two-neutron removal cross sections from these proton-rich nuclei with  $N = 12, 14, 16$  were found to be of the order of 1 mb; similar to those observed in two-proton knockout experiments from the neutron-rich  $sd$ -shell nuclei with  $Z = 12, 14$  [22]. Based on the energetics of the reaction and the observed cross sections, the two-neutron removal processes discussed here appear to proceed by the direct reaction

mechanism.

This work was supported by the U.S. National Science Foundation under Grants No. PHY-0110253 and No. PHY-0244453 and by the United Kingdom Engineering and Physical Sciences Research Council (EPSRC) Grant No. EP/D003628.

\* Present address: RIKEN, Hirosawa 2-1, Wako, Saitama 351-0198, Japan

† Present address: American Science & Engineering, Inc., 829 Middlesex Turnpike, Billerica, MA 01821, USA

‡ Present address: Laboratoire de Physique Corpusculaire, 6 Boulevard du maréchal Juin, 14050 Caen Cedex, France

- [1] P. G. Hansen and J. A. Tostevin, *Annu. Rev. Nucl. Part. Sci.* **53**, 219 (2003).
- [2] A. Navin *et al.*, *Phys. Rev. Lett.* **81**, 5089 (1998).
- [3] D. Bazin *et al.*, *Phys. Rev. C* **57**, 2156 (1998).
- [4] T. Aumann *et al.*, *Phys. Rev. Lett.* **84**, 35 (2000).
- [5] V. Guimarães *et al.*, *Phys. Rev. C* **61**, 064609 (2000).
- [6] A. Navin *et al.*, *Phys. Rev. Lett.* **85**, 266 (2000).
- [7] E. Sauvan *et al.*, *Phys. Lett. B* **491**, 1 (2000).
- [8] V. Maddalena *et al.*, *Rev. C* **63**, 024613 (2001).
- [9] J. Enders *et al.*, *Phys. Rev. C* **65**, 034318 (2002).
- [10] J. A. Tostevin *et al.*, *Phys. Rev. C* **66**, 024607 (2002).
- [11] M. Thoennessen *et al.*, *Phys. Rev. C* **68**, 044318 (2003).
- [12] J. Enders *et al.*, *Phys. Rev. C* **67**, 064301 (2003).
- [13] A. Gade *et al.*, *Phys. Rev. C* **69**, 034311 (2004).
- [14] A. Gade *et al.*, *Phys. Rev. Lett.* **93**, 042501 (2004).
- [15] J. R. Terry *et al.*, *Phys. Rev. C* **69**, 054306 (2004).
- [16] A. Gade *et al.*, *Phys. Rev. C* **71**, 051301(R) (2005).
- [17] J. A. Tostevin, *J. Phys. G* **25**, 735 (1999).
- [18] B. A. Brown, *Prog. Part. Nucl. Phys.* **47**, 517 (2001).
- [19] B. A. Brown, *Phys. Rev. C* **58**, 220 (1998).
- [20] B. A. Brown, W. A. Richter, and R. Lindsay, *Phys. Lett. B* **483**, 49 (2000).
- [21] B. A. Brown, P. G. Hansen, B. M. Sherrill, and J. A. Tostevin, *Phys. Rev. C* **65**, 061601(R) (2002).
- [22] D. Bazin *et al.*, *Phys. Rev. Lett.* **91**, 012501 (2003).
- [23] J. Fridmann *et al.*, *Nature* **435**, 922 (2005).
- [24] J. A. Tostevin, G. Podolyak, B. A. Brown and P. G. Hansen, *Phys. Rev. C* **70**, 064602 (2004).
- [25] D. J. Morrissey *et al.*, *Nucl. Instrum. and Methods Phys. Res. B* **204**, 90 (2003).
- [26] D. Bazin *et al.*, *Nucl. Instrum. Methods Phys. Res. B* **204**, 629 (2003); J. Yurkon *et al.*, *Nucl. Inst. and Meth. Phys. Res. A* **422**, 291 (1999).
- [27] W. F. Mueller *et al.*, *Nucl. Inst. and Meth. A* **466**, 492 (2001).
- [28] A. Obertelli *et al.*, *Phys. Rev. C* **73**, 044605 (2006).
- [29] R. Brun, GEANT3 user guide, technical report DD/EE/84-1, Cern (1987).
- [30] P. D. Cottle *et al.*, *Phys. Rev. Lett.* **88**, 172502 (2002).
- [31] B. A. Brown *et al.*, computer code OXBASH, MSU-NSCL Report No. 524.
- [32] B. A. Brown and B. H. Wildenthal, *Annu. Rev. Nucl. Part. Sci.* **38**, 29 (1988).
- [33] H. Schatz *et al.*, *Phys. Rev. Lett.* **79**, 3845 (1997).
- [34] A. J. Howard *et al.*, *Phys. Rev. C* **1**, 1446 (1970).
- [35] H. Herndl *et al.*, *Phys. Rev. C* **52**, 1078 (1995).
- [36] J. A. Tostevin *et al.*, in preparation (2006).